Optical control of ferroelectric domains: Nanoscale insight on macroscopic observations

Gaurav Vats[#,], Yang Bai[#], Dawei Zhang, Jari Juuti and Jan Seidel[*]*

Gaurav Vats, Dawei Zhang and Prof. Jan Seidel
School of Materials Science and Engineering, University of New South Wales, Sydney NSW 2052, Australia
*Email: g.vats@unsw.edu.au; jan.seidel@unsw.edu.au
Phone: +61 (0)2 9385 4442; Fax: +61 (0)2 9385 6565

Dr. Yang Bai, Prof. Jari Juuti
Microelectronics Research Unit, Faculty of Information Technology and Electrical Engineering, University of Oulu, FI-90014 Oulu, Finland

[#]Authors contributed equally.

Keywords: Optical control, domain walls, lead-free, ferroelectric, photoferroic effect

Domain wall nanoelectronics constitutes a potential paradigm shift for next-generation energy conversion and von-Newman devices.[1] In this context, attempts have been made to achieve energy efficient control over ferromagnetic[2, 3], ferroelectric[4, 5] and ferroelastic[6] domain walls through electric and magnetic fields or applied stress. However, optical control of ferroic domains offers an additional degree of freedom and significant advantages of reduced hysteresis and Joule heating losses by eliminating the physical contacts. Therefore, optically controlled domain walls are likely to unfurl novel opportunities in the regime of nanoelectronics and photonics. Here, we demonstrate reversible optical control of ferroelectric domains and domain walls in a novel band-gap engineered lead-free ferroelectric ceramic ($(K_{0.5}Na_{0.5})NbO_3$-2 mol.% $Ba(Ni_{0.5}Nb_{0.5})O_{3-\delta}$ (KNBNNO)). The optical poling behaves similar to electrical poling (applied

negative bias in this case) and is governed by the bulk ferroelectric photovoltaic. The light acts as a constant current or voltage source in the short and open-circuited conditions, respectively. These induced current/voltages influence the state of polarization and leads to observed nanoscale changes in the material which could also be correlated with the macroscopic observations. This phenomenon could be potentially be observed in several ferroelectric materials if the voltage generated due to the presence of light source is in the range of the switching voltages. Our work establishes a relationship between light-induced macroscopic observations and nanoscale changes in the ferroelectric response, providing fundamental insight and facilitating research into ferroelectric photovoltaics and optoelectronics.

1. Introduction

Ferroelectric materials possess a spontaneous polarization due to non-centrosymmetry in their structure. This spontaneous polarization can be reversibly tuned using external stimuli such as electrical field, strain and/or thermal fluctuation. Warren *et. al.* manifested that it is also possible to tune the state of spontaneous polarization merely by the exposure of light.[7] Fundamental understanding of this mechanism is likely to offer new device prospects especially in optoelectronics and information storage.[5, 8-11] It is to be noted that the photovoltaic effect in ferroelectrics is well known since the 1960s[12-18] and has been investigated for the optical reading of ferroelectric random-access memories[19, 20], photodiodes[21] and photovoltaic[9, 22-28] applications. Current research is focused on developing band-gap tuned ferroelectric materials as their performance is restricted by low mobility of charge carriers and short diffusion lengths.[29-31] Band-gap tuned ferroelectric materials are capable of hosting multiple functionalities (due to ferroelectricity and semiconducting features) which suggest the possibilities of multiple energy conversions (piezoelectric, pyroelectric and photovoltaic) simultaneously. In this context, Bai *et. al.* synthesized a novel band-gap (1.6 eV down from > 4 eV) engineered lead-free ferroelectric composition ($(K_{0.5}Na_{0.5})NbO_3$-2 mol.% $Ba(Ni_{0.5}Nb_{0.5})O_{3-\delta}$ (KNBNNO, or KNN-BNNO)) and demonstrated multiple functionalities (piezoelectric, pyroelectric and photovoltaic effects) and their cumulative effect using this single material.[32-34] $(K_{0.5}Na_{0.5})NbO_3$ (KNN) supports off-

center distortion and is responsible for ferroelectric nature of KNN-BNNO while $Ba(Ni_{0.5}Nb_{0.5})O_{3-\delta}$ (BNNO) controls the electronic states in the gap of parent $(K_{0.5}Na_{0.5})NbO_3$ using oxygen vacancies and Ni^{+2} ions.[29] Simultaneous presence of ferroelectric and semiconducting features makes this composition alluring for photovoltaic applications. In addition, it also provides an opportunity to understand how ferroelectric properties in semiconductors could help in improving the photovoltaic response and vice-versa. In this context, the present study aims to provide an insight into light-induced changes in the ferroelectric behavior of KNN-BNNO. Recent demonstration of light driven switching of nano-domains in $(K_{0.5}Na_{0.5})NbO_3$ also makes it interesting to further explore KNN-BNNO[35].

Light-induced changes in ferroelectrics could persist due to a number of reasons such as (i) localized heating assisted diffusion of alkali element (as in $LiNbO_3$) and oxygen vacancies[36], (ii) change in oxidation state of the central atom (e.g. in $BaTiO_3$)[37] and (iii) Jahn Teller distortions due to light-induced pyroelectric current or charge injection in the conduction band (as in SbSI)[12, 18]. Warren *et. al.* suggested that similar to electrical and thermal fluctuations, an exposure to light involves "*locking domains by electronic charge trapping at domain boundaries"*.[7] It is well known that the macroscopic polarization of a ferroelectric is an intrinsic feature of its inherent domains. Therefore, any change in macroscopic behavior could be attributed to nanoscale changes in the ferroelectric domains. Moreover, it is interesting to know that which of the three mechanisms is responsible for optical behavior of KNN-BNNO. Hence, we investigated light dependent nanoscale changes in KNN-BNNO using a homemade photoelectric atomic force microscopy (see the Method section and supplementary information for details). In this study, Piezo-response Force Microscopy (PFM) and Kelvin Probe Force Microscopy (KPFM) measurements have been performed and the obtained results have been correlated with the macroscopic observations. The same results have been used to confirm the achievement of additional control over ferroelectric behaviour by the exposure of light. An understanding thus attained would be helpful in developing semiconducting ferroelectrics based optoelectronic devices with additional functionalities. Moreover, it will stimulate the development of novel device mechanisms to achieve optical control over ferroelectricity and ferroelectric domain walls by effective utilization of the associated semiconducting material characteristics.

2. Results and discussion

Firstly, light dependent temporal piezo-response force microscopy (PFM) was performed to understand the nanoscale effects of light on KNN-BNNO. Out-of-plane phase images and PFM amplitude were acquired after every 10 minutes for 100 minutes of continuous exposure to a monochromatic DC laser source of wavelength 405 nm (see supporting Figure S 1.1). Afterwards, the laser was turned off and PFM signal was recorded for another 100 minutes in dark (shown in supporting Figure S 1.2). Figure 1 (a)-(f) presents the nanoscale movement of domains and domain walls with continuous exposure to light and the reversal on turning the light off. The changes are highlighted by the dotted white boxes. Interestingly, most of the domains returned to their original position with a few exceptions. These exceptions could be attributed to the difference of the potential energy of the unrecoverable domain walls from those of the recoverable.[38] For these unrecoverable domain walls, the exposure of light might have given enough energy to fully overcome the potential between out-of-plane and in-plane domain walls or defects. When the light was turned off, these stable domain walls could not fully reverse to the initial status, because they had to overcome the same potential, but no extra energy was obtained and allowed them to do so. Another intriguing observation is the change in contrast of domains shown in Figure 1 (a) and (b). This can be more clearly observed in supporting Figures S 1.1 and S 1.2 which signify a change in the phase difference of the domains with up and down polarizations. In order to elucidate this, PFM amplitude of domains with outward polarization are plotted in Figure 1 (g) and the fractional change in domain area (calculated from out-of-plane bright domains) is unfolded in Figure 1 (h) (shaded area represents the time corresponding to the laser exposure). Both trends complement each other. It can be established that an exposure to a laser source leads to the increase in piezo-response of the domains to a maximum value followed by domain relaxation at a point with higher piezo-response in contrast to the dark condition. Such behavior can be interpreted as light-induced ferroelectric poling. Furthermore, it is found that the area fraction decreases on exposure to the laser source in comparison to the dark condition followed by a sudden jump corresponding to the maximum PFM amplitude and finally leading to the minimal domain area of the relaxed condition (Figure 1(h)). It is to be noted that the piezo-response amplitude of the first image acquired in dark condition is significantly different from the image acquired after 100 minutes of turning the laser off. This is because the sample is very sensitive to the full spectrum of the visible light including the white light in the

room and was not at a fully relaxed condition at the beginning of the experiment. To confirm this, similar experiments were carried out at several locations (See Figure S 1.3 for light induced changes on a larger area) with different pre-experiment dark resting time, but it was difficult to estimate the actual dark condition response. Therefore, a confirmation of optical poling of ferroelectric domains was also performed macroscopically by exposing an unpoled sample with negligible piezoelectric constant to white light for 8 hours. Post-exposure piezo-response (piezoelectric charge coefficient d_{33}) of the sample raised to 4 pC/N, which also confirms the optical control of polarization state of the ferroelectric domains. It is to be noted that optical poling of ferroelectric domains depends on the intensity of incident radiation and the exposure time. In the present case, the illumination source only helped in partial and reversible poling of the sample, not a complete poling of the sample, which could lead to very high d_{33} (200 pC/N)[32] values. The light induced change in polarization state was also confirmed by the difference in the piezo-response of the samples electrically poled in dark and light (405 nm) conditions for same time (30 mins) and applied electric field (10 kV cm^{-1}). The sample poled in dark showed a piezo-response of 25 pC/N while the sample poled in light illustrated 37 pC/N. Both these d_{33} values were measured in dark. Since the d_{33} is dependent on the polarization of the material, it can be concluded macroscopically as well as at the nanoscale that light can be used to achieve optical control over ferroelectric polarization in KNN-BNNO.

In addition to the results shown above, reversible control over domain walls is unveiled in Figure 1 (i)-(k). A clear reversible and fully reproducible collapse and splitting of two domain walls can be observed on exposure to laser and on turning it off, respectively. The understanding attained so far concludes optical control of domain walls and light assisted electrical poling. However, it is difficult to measure the exact difference in the domain and domain wall velocities on exposure to light as it is a dynamic process and is continuously occurring during the PFM scans. This could be clearly observed from the squared areas in Figure S 1.1. From our measurements, domain walls velocities as high as 1 nm/minute have been observed (e.g. seen in Fig. 1 (i-k)). In principle, a constantly applied DC bias will lead to the state of maximum polarisation until an equilibrium is achieved. Afterwards, the macroscopic polarisation, which is a resultant of the interaction between polarisations, becomes constant. Nevertheless, this constant change in macroscopic observation does not guarantee an equilibrium at the nanoscale. The light induced maximum polarisation in two adjacent domains may keep on interacting with each other

for very long times in contrast to the macroscopic equilibrium time (see the fluctuation in encircled domain in Figure S 1.1). On the contrary, the change in macroscopic polarisation with light (shown in Figure 2 (a)) was found to be instantaneous and stable over long periods of time (no change was observed even after 1 hr). This means that the light induced nanoscale changes instantaneously provide the most significant macroscopic fluctuation in polarisation. Thereafter, longer exposure times (~8 hrs) lead to partial poling of the sample which supports the argument of continuous long-term interaction of domains until a state of equilibrium is achieved. Intriguingly, this also suggests that light dependent nanoscale and macroscopic changes could be utilised separately for distinct device applications. An understanding of the physics behind this phenomena could help to achieve a precise control over domain walls that can be used to prepare an optically controlled ferroelectric counterpart of spin polarized race-track memories[39] and many other advanced optoelectronic devices.

Aforementioned observations in KNN-BNNO could be distinguished from localized heating and pyroelectric effect by temperature dependent *P-E* loops displayed in Figure S 2.1 in the supporting information. A nominal change (< 2μC/cm^2) in polarization over the broad temperature range (20^{0}C to 155^{0}C) ruled out the possibility of localized heating and pyroelectric effect. All of the nanoscale experiments were performed at room temperature and the localized temperature change corresponding to the wavelength of 405 nm was found to be 0.5^{0}C (direct measurement using a thermocouple). Furthermore, nanoscale electrical poling experiments were performed to have an insight on the light dependent behavior. It is found that the sample is quite sensitive to the electrical poling and even small voltages (both AC and DC) of 0.5 V are sufficient to cause a change in ferroelectric domains. Therefore, a significantly higher DC bias of -6 V was chosen for the electrical poling experiment while PFM was performed with an AC bias of 0.2 V. The experiments were performed under the same parameters as during optical poling in full dark condition. Post-poling PFM images acquired at constant intervals for 60 minutes suggest that the electrical poling using negative bias behaved analogous to the optical poling (see results depicted in supporting Figure S 3.1). The domains returned to their original position in around 30 minutes and attained stability afterwards. This means that the light is acting as a constant current source for the material as all experiments were performed in the short circuit conditions. The same phenomenon was confirmed using light-dependent (λ=405 nm) short circuit current measurement as shown in Figure 3. Figure 3 (a) shows the photocurrent measured

macroscopically with Cr-Au and ITO electrodes. The sample is behaving as a photo-transistor/photo-detector – a device where merely by switching light on and off a remarkable change in short circuit current density could be observed. Similar behavior was observed in the full visible light range but with a comparatively lower photocurrent density (See Figure S 4.1). The photocurrent was also observed at the nanoscale (Figure 3 (b)) with Cr-Au electrode on one side of the sample and AFM tip acting as the electrode on the other side. However, a small AC bias of 0.2 V was applied for nanoscale photocurrent measurement for the following two reasons:

(i) The photocurrent values fall below the detection range of the instrument as the electrode size (AFM tip contact ~ 10 nm) is very small and, therefore, it becomes difficult to detect the short-circuit photocurrent corresponding to λ=405 nm. The photocurrent for wavelengths >405 nm is even smaller and therefore the nanoscale photocurrents corresponding to them were not recorded.

(ii) All PFM measurements were performed with an AC bias of 0.2 V. So, it becomes essential to understand the photocurrent behavior under the same conditions.

Analogous to macroscopic photocurrent density a significant difference in the nanoscale photocurrent density was observed merely by changing the light intensity. This means that the small-applied AC voltage only helped in scaling the photocurrent density and tuning the sensitivity of the instrument. The nanoscale photocurrent measurement clearly shows that there is a huge difference in rise and decay times of the photocurrent that can be estimated using exponential fitting ($I = I_0 + A_1 e^{\pm(t-t_0)/\tau}$). τ is the photocurrent rise and decay constant, found to be 12 s and 72 s, respectively. This difference in rise and decay time explicates why the domain movement on exposure is faster in contrast to the reversal in dark (note that the maximum nanoscale change is observed in the first 10 minutes of exposure (see S 1.1 (a)-(b)) while a significant reversal is observed in the first 30 minutes after turning the laser off (See Figure S 1.2 (a)-(d)). In addition to this, the change in current density was also recorded for positive (Figure 3 (c)) and negative (Figure 3 (d)) bias of 1 V which was chosen to show significant difference in the current density with the least possible influence of the switching current. Similar trends of change in current density were observed at different locations on the sample when measured (AFM tip was placed) at up and down domains and their interfaces.

Intriguingly, the direction of the increase in current density for applied negative bias is found to be the same as of the photocurrent and is opposite to the direction of increase in the current density for applied + 1 V. This helps in establishing the fact that the sample supports a particular type of charge carrier, which is obvious for any semi-conducting material. Having established this fact, an understanding of the shrinking of bright (up) and expansion of dark (down) domains on exposure to illumination could be made. The orientation/polarisation of domains is due to specific alignment of dipoles in a region. Change in concentration of charge carriers in the material influences the orientation of the dipoles and hence the state of polarisation. That is why up domains are favoured under illumination and a reduction in charge carrier concentration in dark condition leads to the reversal of optically polarised domains.

Importantly, it has been reported that a change in short-circuit current can cause charge injection leading to the tuning of the coercive field.[40] The maximum electric field associated with induced current injection can be calculated using the following equation[40-42]:

$$E_{max} = 0.4\left(\frac{I_{SC}}{\pi\theta\mu\varepsilon_0\varepsilon_r}\right)^{1/2}\left(\frac{1}{r}\right)^{1/2} \quad (1)$$

E_{max} is the electric field associated with the current injection (short circuit current (I_{SC}) in this case). r is the electrode area, θ is a parameter for trapping effects in the shallow band gap regions, ε_0 and ε_r are the vacuum and relative permittivity of the material. The equation could be rearranged as follows to estimate the change in electric field with variation in short circuit current:

$$\frac{E_{Dark}}{E_\lambda} = \left(\frac{\varepsilon_\lambda I_{SC,Dark}}{\varepsilon_{Dark} I_{SC,\lambda}}\right)^{1/2} \quad (2)$$

$$\frac{E_{Dark}}{\left(\frac{\varepsilon_\lambda I_{SC,Dark}}{\varepsilon_{Dark} I_{SC,\lambda}}\right)^{1/2}} = E_\lambda \quad (3)$$

Here, it is to be noted that the change in relative permittivity for KNN-BNNO at higher frequencies (600-900 kHz) is 70%, as shown in Figure 2 (d). The PFM measurements were also carried out in the same frequency range. This relation suggests that in the present case $E_{\lambda=405} \sim 5E_{Dark}$. θ is assumed to be constant but is likely to change under experimental

conditions, so the value may vary. The change in relative permittivity (shown in Figure 2 (b)) can be explained through the following relationship:

$$P=\varepsilon_r\chi E \quad (4)$$

here, P= polarization; χ= dielectric susceptibility; E= applied electric field. Light-induced non-linear reduction in the real part of dielectric constant at low frequencies (see Figure 2 (b) and (d)) means a small increase in polarization in contrast to the net applied field (a combination of the applied electric field $(E_{Applied})$ and light induced enhanced electric field (E_λ);$P/E= P/(E_{Applied}+ E_\lambda) = \varepsilon_r\chi)$ whereas, χ governs the frequency dependence of this behavior. A cumulative effect of light induced electric and depolarization field will thus govern the material behavior and optical control over ferroelectric behavior.

Similar to nanoscale experiments, illumination during the macroscopic measurements cause charge injection. Due to this charge injection a change in the state of polarization is expected as noticed in *P*-*E* loop data (measured at 1 Hz) shown in Figure 2 (a). Nominal change in dielectric losses at low frequencies (<100 kHz) shows that the increase in polarization and corresponding decrease in dielectric constant at low frequencies must primarily originate from the optical poling of the ferroelectric domains. The same is also supported by the nanoscale and piezoelectric measurements. However, the dielectric losses under cumulative effect of light and applied electric field will be different. Therefore, the increase in polarization at all other points except E=0 must be a combination of light assisted polarization of the material and the leakage current induced by the cumulative effect of applied electric field and photocurrent due to the nature of the measurement process. Nevertheless, it is difficult to distinguish between the two based on the macroscopic measurements, the fact that sample is polarized under light can be unambiguously accepted. Interestingly, the light dependent increase in remnant polarization in KNN-BNNO is analogous to observations in a few recent studies[8, 11, 30, 31] but is not commonly observed in ferroelectrics[7]. Remnant polarization decreases on exposure to ultraviolet light in classical ferroelectrics such as (Pb,La)(Zr,Ti)O_3.[7] This difference could again be explained using equation 4 and the optical behavior of ferroelectrics can be classified as type (i) or type (ii) (as introduced above) similar to the temperature dependant changes (decrease or increase) in polarization.[43]

Another method to confirm light induced change in surface potential (or induced electric field) is Kelvin Probe Force Microscopy (KPFM). In our experiments, the tip was maintained at a constant height of 10 nm from the surface of the sample and KPFM was performed. Figure 4 (a) shows the topography of the area under investigation. The sample was initially (first 200 nm distance in the x-direction) maintained at the full dark condition and was then consecutively exposed to the light of wavelengths 700nm, 600nm, 500nm and 405nm for equal scanning areas. The contact potential difference (CPD) of the line shown in Figure 4 (a) is plotted in Figure 4 (b) (white line with circular symbols) while the background shows the KPFM mapping of the area in Figure 4 (a). Figure 4 (b) clearly illustrates that light corresponding to 405nm creates the maximum difference in the surface potential of KNN-BNNO while the CPD for other wavelengths is significantly low. This is in line with the macroscopic photocurrent measurement. Further, to elucidate the potential rise and decay time of the surface potential, KPFM was performed on the same area but with different parameters (for longer scanning time and more data points) to observe time-dependent variation in CPD (see supplementary section S5 for experimental details). Figure 4 (c) shows the KPFM mapping of the sample area while the CPD profiles corresponding to the line marked in Figure 4 (c) are drawn in Figure 4 (d). A sharp increase in CPD could be clearly observed for all wavelengths while the time for decay is relatively quite high. The decay could further be categorised in sudden (zone (I)) and slow decay (zone (II)) zones. This shows the ability of KNN-BNNO to allow and maintain charge traps for a longer time than the light-induced poling in unpoled samples. Such ability is a prerequisite for the non-contact optical reader of a ferroelectric RAM[19,20].

The KPFM and photocurrent measurements can help us concluding that the light induces charge carriers on the surface of the material. The semiconducting nature of KNN-BNNO further help in migration of these charge carriers towards the bottom electrode and finally a constant potential is maintained across the two electrodes. This potential influence the state of polarization in the material, which leads to the movement of the domains and domain walls. Consequently, it must result in some structural changes in the material such as migration of oxygen vacancies or a tetragonal or octahedral shift along with the increased dielectric losses in the material (See Figure 2 (c) for dielectric losses). It is to be noted that the light dependent *P-E* loops were captures at low frequencies (1 Hz) where the losses are quite low in contrast to the losses at the higher frequencies (>600kHz) which were used while performing PFM. Therefore,

there is a good possibility that the increase in polarization is a cumulative effect of changes induced in domains (which are fundamentally related to the structure of the material) and the losses. The same is also supported for the macroscopic d_{33} measurements. However, it is difficult to distinguish between the two as all ferroelectric characterizations involve either electrical contacts or a light/energy source. Undoubtedly, the light-induced surface charge is compensated by the movement of the domain walls and change in state of polarization of domains at least till the Debye length which means that there must be some structural changes and thus, the increase in polarization can not be merely an artefact/loss. Quantitative measurement of the contribution of light induced structural changes and losses towards polarization is an open-ended question but irrespective of this, both the light induced dielectric losses and the structural changes can be utilized to achieve optical control of ferroelectric domains.

3. Conclusions

Experiments described above suggest that the exposure to light changes the surface potential of the sample as the light acts as a constant current source in short circuit condition. The charge carriers injected through the surface of the material polarize the dipoles similar to an applied electric field. The material is behaving as a phototransistor; therefore, it is likely that the charges are distributed throughout the sample thickness, which is also confirmed by the macroscopic piezoresponse noticed after 8 hours of exposure to the white light. The same can also be conceived from the light dependent increase in remnant polarization. However, the possibility of diffusion of oxygen vacancies or current channeling through defects leading to macroscopic change in polarization can not be completely ruled out. The effect is likely to be irreversible or dynamically slow if only ionic defects such as oxygen vacancies are responsible for this kind of behavior. Since $(K_{0.5}Na_{0.5})NbO_3$ supports off-center distortion and $Ba(Ni_{0.5}Nb_{0.5})O_{3-\delta}$ controls the electronic states in the gap of parent $(K_{0.5}Na_{0.5})NbO_3$ using oxygen vacancies and Ni^{+2} ions, it could be concluded that the light affects the number of charge carriers in $Ba(Ni_{0.5}Nb_{0.5})O_{3-\delta}$ which eventually leads to structural changes in KNN-BNNO. Thus, the light-induced reversible

poling of ferroelectric domains and domain walls' movement in KNN-BNNO are due to a combined effect of fluctuations in semiconducting response aided by the non-centrosymmetric distortion caused by the light. Our main finding is that light behaves as a virtual current/voltage source through the photovoltaic effect. If the switching voltages of the sample are in the range of the electric field induced by the incident light, then it could be possible to achieve optical control over domains and domain walls in several ferroelectric materials. We hope that the understanding gained here will help the creation of novel photonic and optoelectronic devices based on ferroelectrics.

Experimental Section

Sample fabrication: $(K_{0.49}Na_{0.49}Ba_{0.02})(Nb_{0.99}Ni_{0.01})O_{2.995}$ (KNN-BNNO) ceramics were fabricated via the solid-state reaction method, from the starting reactants of K_2CO_3 (≥ 99 %, J. T. Baker, USA), Na_2CO_3 (≥ 99 %, Sigma-Aldrich, USA), $BaCO_3$ (99.98 %, Aldrich Chemistry, USA), NiO (99.999 %, Aldrich Chemistry, USA) and Nb_2O_5 (99.9 %, Aldrich Chemistry, USA). As the reactants are hygroscopic, they were dried at 220 ˚C for over 4 hours before weighing, in order to ensure the correct stoichiometry. The precise weighing was carried out with an electronic balance of 0.01 mg readability and 1 mg accuracy (ES 225SM-DR, Precisa, Dietikon, Switzerland). The weighed reactants were mixed in a ZrO_2 jar on a planetary ball mill (Pulverisette 6, Fritsch, Idar-Oberstein, Germany). ZrO_2 balls (3 mm diameter) and ethanol were used as the milling media. The mixing went for 6 hours, followed by drying at 80 ˚C. The one-step calcination was carried out at 850 ˚C for 4 hours in air. The calcined powder was milled again for 12 hours with the same procedure presented above. After drying at 80 ˚C, 8.8 wt.% of the binder (3.3 wt.% polyvinyl alcohol dissolved in deionized water) was added and mixed with the powder. The mixture was uniaxially pressed at 62 MPa into 14.5 mm diameter discs. Following burning off the binders at 500 ˚C for 10 hours with a slow ramping rate of 1 ˚C min^{-1}, the discs were subsequently sintered at 1165 ˚C for 2 hours on Pt foil. During sintering, the samples were placed in a covered alumina crucible and buried by sacrificial powder of the same composition to help inhibit the volatilization of potassium. After sintering samples were polished

with P1200 silicon carbide abrasive paper (Eco-Wet, KWH Mirka Ltd., Finland) cooled by ethanol on a 3 μm grain-sized plate (MD Dur, Struers, Denmark) with diamond suspension (DiaPro Mol B3, Struers, Denmark), and on a 1 μm grain-sized plate (MD Nap, Struers, Denmark) with diamond suspension (DiaPro Nap B1, Struers, Denmark). An average surface roughness of 50-60 nm was obtained. The samples were finally 100-150 μm thick. In addition, a 200 nm thick ITO (indium tin oxide) electrode was coated on one side of each sample whilst a 220 nm thick metal (20 nm Cr and 200 nm Au, Au on top) electrode was put on the other side.

Macroscopic characterization: A ferroelectric test system (Precision LCII, Radiant Technologies, Inc., USA) was used to measure ferroelectric hysteresis (*P*-*E*) loops. The temperature was controlled by silicone oil heated on a hot plate. The d_{33} values were measured with a Berlincourt piezoelectric meter (YE2730A, APC International Ltd., USA). A source meter (2450, Keithley, USA) was used to measure photocurrents. Lasers (OBIS LX/LS series, Coherent, USA) with different wavelengths were used as the light sources. The wavelength/maximum power/beam diameter at $1/e^2$ were 405 nm/50 mW/0.8±0.1 mm, 552 nm/20 mW/0.7±0.05 mm and 660 nm/100 mW/0.9±0.1 mm, respectively. A 14 W white light energy saving fluorescent lamp which illuminated the entire sample surface with an intensity of ~12.5 mW cm^{-2} was used to test light-induced poling. The intensity of the white light was measured with an S120C silicon photodiode detector integrated with a PM100D optical power and energy meter (Thorlabs, Germany). The incident light was shaded on the ITO electrodes.

Nanoscale measurements: A Cr-Au electrode was deposited on one side of the sample while the other surface was left uncoated and was then further polished using a 0.25 μm diamond suspension (DiaPro Nap 1/4, Struers, Denmark). The peak-to-peak surface roughness was reduced to 5-10 nm. The disc samples were laser-cut into 5 mm x 5 mm square samples for the convenience of nanoscale measurements. AFM (Atomic Force Microscopy), PFM (Piezoresponse Force Microscopy) and KPFM (Kelvin-probe Force Microscopy) measurements were performed in the dark using a customized AIST-NT Smart SPM system and a Fianium Whitelase supercontinuum laser. The light source with variable wavelengths (405 nm, 500 nm, 600 nm and 700 nm) was used to illuminate the samples. The switching voltages were initially determined by the electrical poling experiments. An AC bias of 0.5 V was found to be able to cause partial domain switching in the samples. Therefore, an optimized AC bias of 0.2 V was

applied between the bottom Cr-Au electrode and the conductive AFM tip (Platinum coated NSC35/PT probes from MikroMasch) when carrying out the light induced temporal PFM measurements. A non-contact mode with a lift height of 10 nm was chosen for the KPFM measurements. Initially, a smooth area was found and then a constant lift height of 10 nm was maintained between the AFM tip and the sample surface. Incident light with different wavelengths was used in KPFM measurements.

Supporting Information

Supporting Information is available from the Wiley Online Library or from the author.

Acknowledgement

We acknowledge support by the Australian Research Council (ARC) through Discovery Grants. Y.B. acknowledges funding from the European Union's Horizon 2020 research and innovation program under the Marie Sklodowska-Curie grant agreement number 705437. The authors also acknowledge the Centre of Microscopy and Nanotechnology of University of Oulu for the use of their facilities and for the fabrication of electrodes.

References

1. G. Catalan, J. Seidel, R. Ramesh, J. F. Scott, *Reviews of Modern Physics* **2012**, *84*, 119.
2. M. Yamanouchi, D. Chiba, F. Matsukura, H. Ohno, *Nature* **2004**, *428*, 539.
3. Y.-H. Chu, L. W. Martin, M. B. Holcomb, M. Gajek, S.-J. Han, Q. He, N. Balke, C.-H. Yang, D. Lee, W. Hu, *Nature Materials* **2008**, *7*, 478-482.
4. S. M. Park, B. Wang, S. Das, S. C. Chae, J.-S. Chung, J.-G. Yoon, L.-Q. Chen, S. M. Yang, T. W. Noh, *Nature Nanotechnology* **2018**, 1.
5. F. Rubio-Marcos, A. Del Campo, P. Marchet, J. F. Fernández, *Nature Communications* **2015**, *6*, 6594.
6. V. Nagarajan, A. Roytburd, A. Stanishevsky, S. Prasertchoung, T. Zhao, L. Chen, J. Melngailis, O. Auciello, R. Ramesh, *Nature Materials* **2003**, *2*, 43-47.
7. W. Warren, D. Dimos, B. Tuttle, G. Pike, R. Schwartz, P. Clews, D. McIntyre, *Journal of Applied Physics* **1995**, *77*, 6695-6702.
8. F. Rubio-Marcos, D. A. Ochoa, A. Del Campo, M. A. García, G. R. Castro, J. F. Fernández, J. E. García, *Nature Photonics* **2018**, *12*, 29.
9. J. Chakrabartty, C. Harnagea, M. Celikin, F. Rosei, R. Nechache, *Nature Photonics* **2018**, *12*, 271.

10. R. Guo, L. You, Y. Zhou, Z. S. Lim, X. Zou, L. Chen, R. Ramesh, J. Wang, *Nature Communications* **2013**, *4*, 1990.
11. A. Makhort, F. Chevrier, D. Kundys, B. Doudin, B. Kundys, *Physical Review Materials* **2018**, *2*, 012401.
12. V. Fridkin, I. Groshik, V. Lakhovizkaya, M. Mikhailov, V. Nosov, *Applied Physics Letters* **1967**, *10*, 354-356.
13. P. S. Brody, F. Crowne, *Journal of Electronic Materials* **1975**, *4*, 955-971.
14. A. Glass, D. Von der Linde, D. Auston, T. Negran, *Journal of Electronic Materials* **1975**, *4*, 915-943.
15. G. Chanussot, V. Fridkin, G. Godefroy, B. Jannot, *Applied Physics Letters* **1977**, *31*, 3-4.
16. V. Fridkin, *Applied Physics* **1977**, *13*, 357-359.
17. V. M. Fridkin, B. Popov, *Soviet Physics Uspekhi* **1978**, *21*, 981.
18. V. M. Fridkin, *Photoferroelectrics*. (Springer Science & Business Media, 1979).
19. P. S. Brody, US Patent No. 4,103,341 (1978).
20. S. Thakoor, A. P. Thakoor, US Patent No. 5,206,829 (1993).
21. T. Choi, S. Lee, Y. Choi, V. Kiryukhin, S.-W. Cheong, *Science* **2009**, *324*, 63-66.
22. J. E. Spanier, V. M. Fridkin, A. M. Rappe, A. R. Akbashev, A. Polemi, Y. Qi, Z. Gu, S. M. Young, C. J. Hawley, D. Imbrenda, *Nature Photonics* **2016**.
23. N. Faraji, C. Ulrich, N. Wolff, L. Kienle, R. Adelung, Y. K. Mishra, J. Seidel, *Advanced Electronic Materials* **2016**, *2*, 1600138.
24. J. Wang, G. Liu, D. Sando, V. Nagarajan, J. Seidel, *Applied Physics Letters* **2017**, *111*, 092902.
25. J. Seidel, L. M. Eng, *Current Applied Physics* **2014**, *14*, 1083-1091.
26. J. Seidel, S.-Y. Yang, E. Alarcòn-Lladò, J. Ager III, R. Ramesh, *Ferroelectrics* **2012**, *433*, 123-126.
27. N. Faraji, R. Adelung, Y. Mishra, J. Seidel, *Nanotechnology* **2017**, *28*, 405701.
28. S. Yang, J. Seidel, S. Byrnes, P. Shafer, C.-H. Yang, M. Rossell, P. Yu, Y.-H. Chu, J. Scott, J. Ager III, *Nature Nanotechnology* **2010**, *5*, 143.
29. I. Grinberg, D. V. West, M. Torres, G. Gou, D. M. Stein, L. Wu, G. Chen, E. M. Gallo, A. R. Akbashev, P. K. Davies, *Nature* **2013**, *503*, 509-512.
30. H. Borkar, V. Rao, S. Dutta, A. Barvat, P. Pal, M. Tomar, V. Gupta, J. Scott, A. Kumar, *Journal of Physics: Condensed Matter* **2016**, *28*, 265901.
31. H. Borkar, M. Tomar, V. Gupta, R. S. Katiyar, J. Scott, A. Kumar, *Materials Research Express* **2017**, *4*, 086402.
32. Y. Bai, P. Tofel, J. Palosaari, H. Jantunen, J. Juuti, *Advanced Materials* **2017**, 1700767.
33. Y. Bai, T. Siponkoski, J. Peräntie, H. Jantunen, J. Juuti, *Applied Physics Letters* **2017**, *110*, 063903.
34. Y. Bai, G. Vats, J. Seidel, H. Jantunen, J. Juuti, *Advanced Materials* **2018**.
35. F. Rubio-Marcos, A. Del Campo, R. E. Rojas-Hernandez, M. O. Ramírez, R. Parra, R. U. Ichikawa, L. A. Ramajo, L. E. Bausá, J. F. Fernández, *Nanoscale* **2018**, *10*, 705-715.
36. H. Steigerwald, M. Lilienblum, F. Von Cube, Y. Ying, R. Eason, S. Mailis, B. Sturman, E. Soergel, K. Buse, *Physical Review B* **2010**, *82*, 214105.
37. S. Abel, T. Stöferle, C. Marchiori, C. Rossel, M. D. Rossell, R. Erni, D. Caimi, M. Sousa, A. Chelnokov, B. J. Offrein, *Nature Communications* **2013**, *4*, 1671.
38. D. Damjanovic, *Reports on Progress in Physics* **1998**, *61*, 1267.
39. S. S. Parkin, M. Hayashi, L. Thomas, *Science* **2008**, *320*, 190-194.
40. M. M. Yang, M. Alexe, *Advanced Materials* **2018**, *30*, 1704908.
41. M. Lampert, A. Many, P. Mark, *Physical Review* **1964**, *135*, A1444.
42. M. A. Lampert, P. Mark, *Current injection in solids*. (Academic Press, 1970).
43. G. Vats, A. Kumar, N. Ortega, C. R. Bowen, R. S. Katiyar, *Energy & Environmental Science* **2016**, *9*, 1335-1345.

Figures

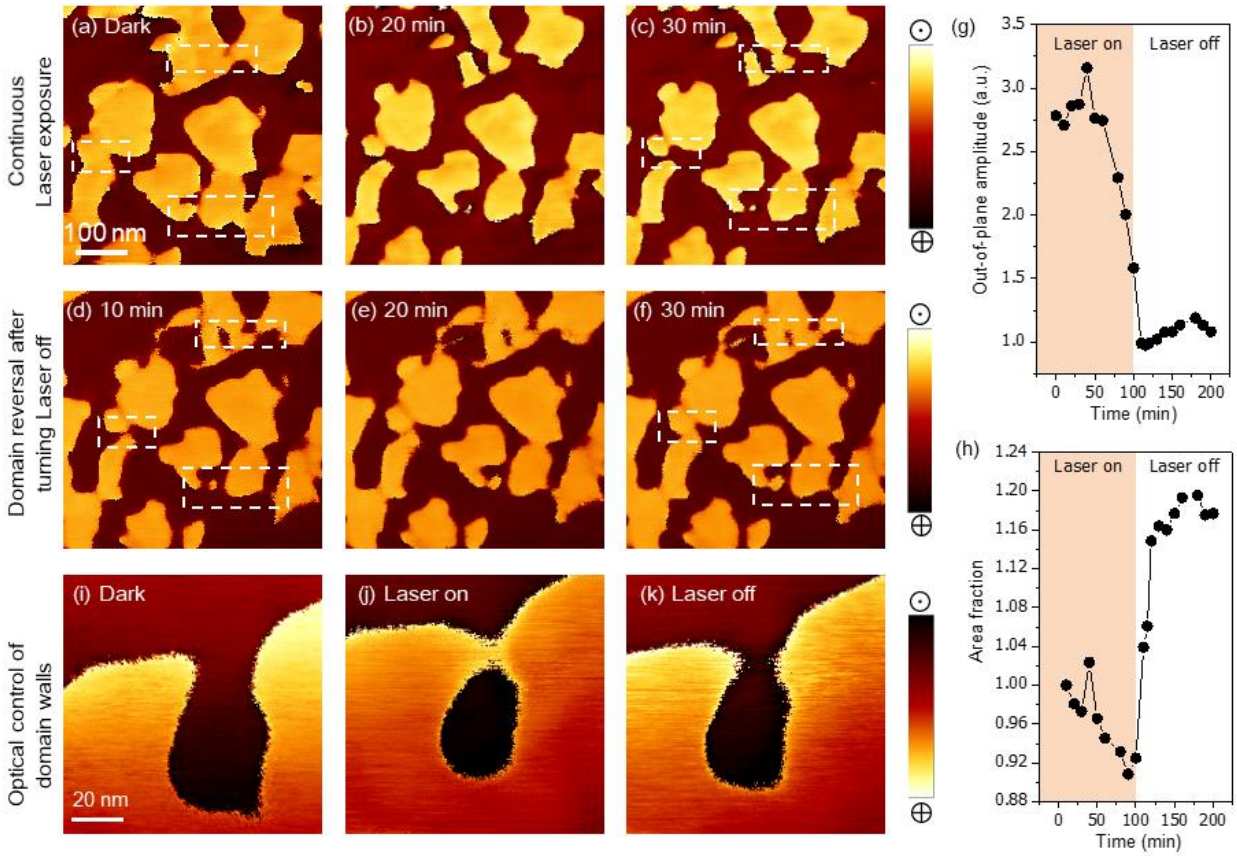
Continuous Laser exposure
(a) Dark
(b) 20 min
(c) 30 min
100 nm
Domain reversal after turning Laser off
(d) 10 min
(e) 20 min
(f) 30 min
Optical control of domain walls
(i) Dark
(j) Laser on
(k) Laser off
20 nm
(g)
Laser on
Laser off
Out-of-plane amplitude (a.u.)
Time (min)
(h)
Laser on
Laser off
Area fraction
Time (min)

Figure 1: Light dependent out of plane piezoresponse force microscopy (PFM). Phase images acquired (a) under dark, after (b) 20 minutes and (c) 30 minutes of continuous exposure to a laser of 405 nm wavelength. Images acquired after (d) 10 minutes, (e) 20 minutes and (f) 30 minutes of laser off, respectively. Change in contrast indicates the localized change in piezoresponse. Light induced change in PFM amplitude is highlighted in (g) while the average fraction change in domain area is plotted in (h). (i)-(k) show the magnified view of domain wall motion corresponding to dark, laser exposure and post laser exposure state. (Note: the notation of up and down domains is different for Figure (a)-(f) and (i)-(k) just to have better presentation).

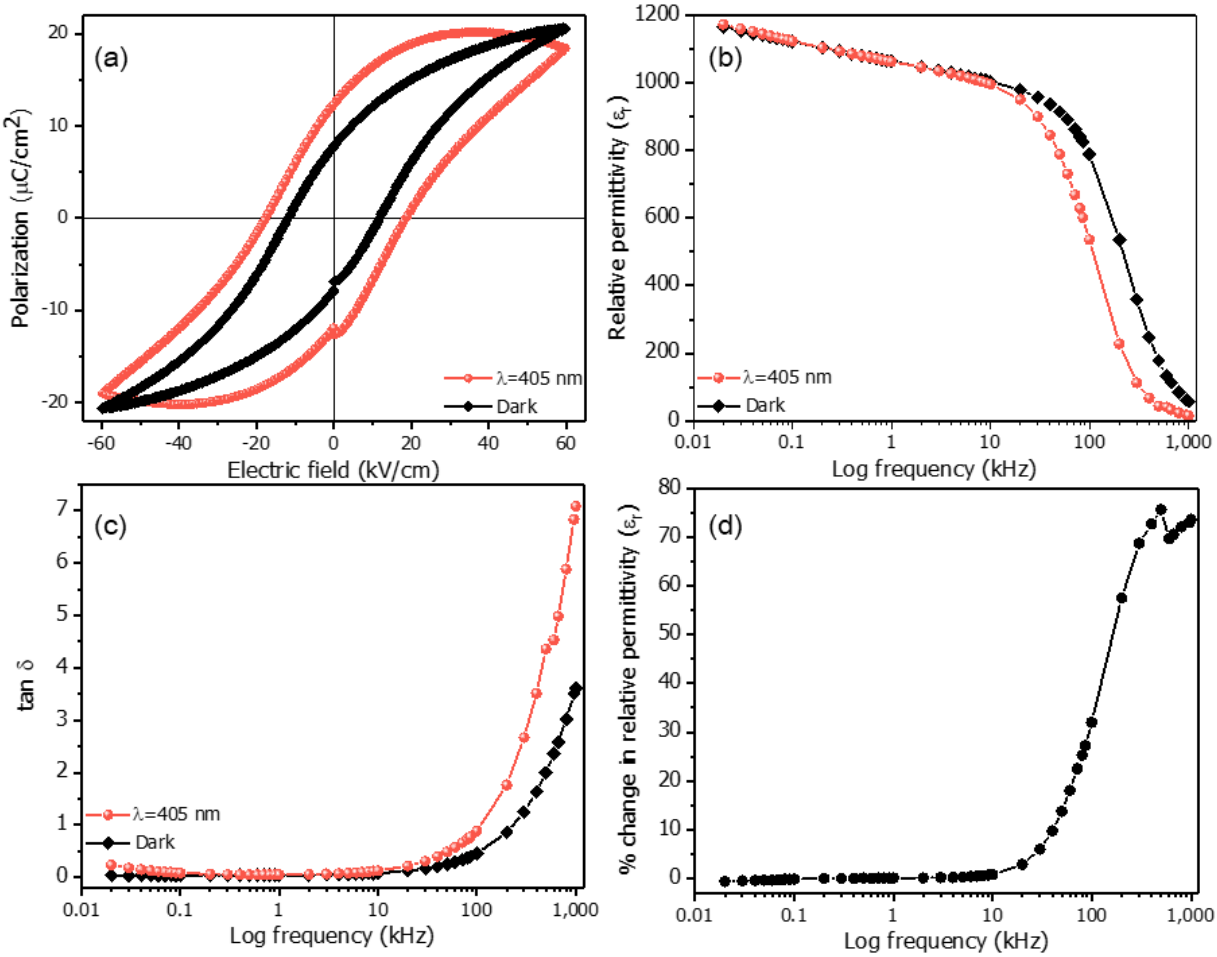

Figure 2: Light-induced changes in ferroelectricity. (a) Ferroelectric hysteresis (*P*-*E*) loops (measured at 1 Hz), (b) frequency dependence of relative permittivity, (c) dielectric losses as a function of log frequency and (d) the relative change in relative permittivity measured in dark and illuminated conditions.

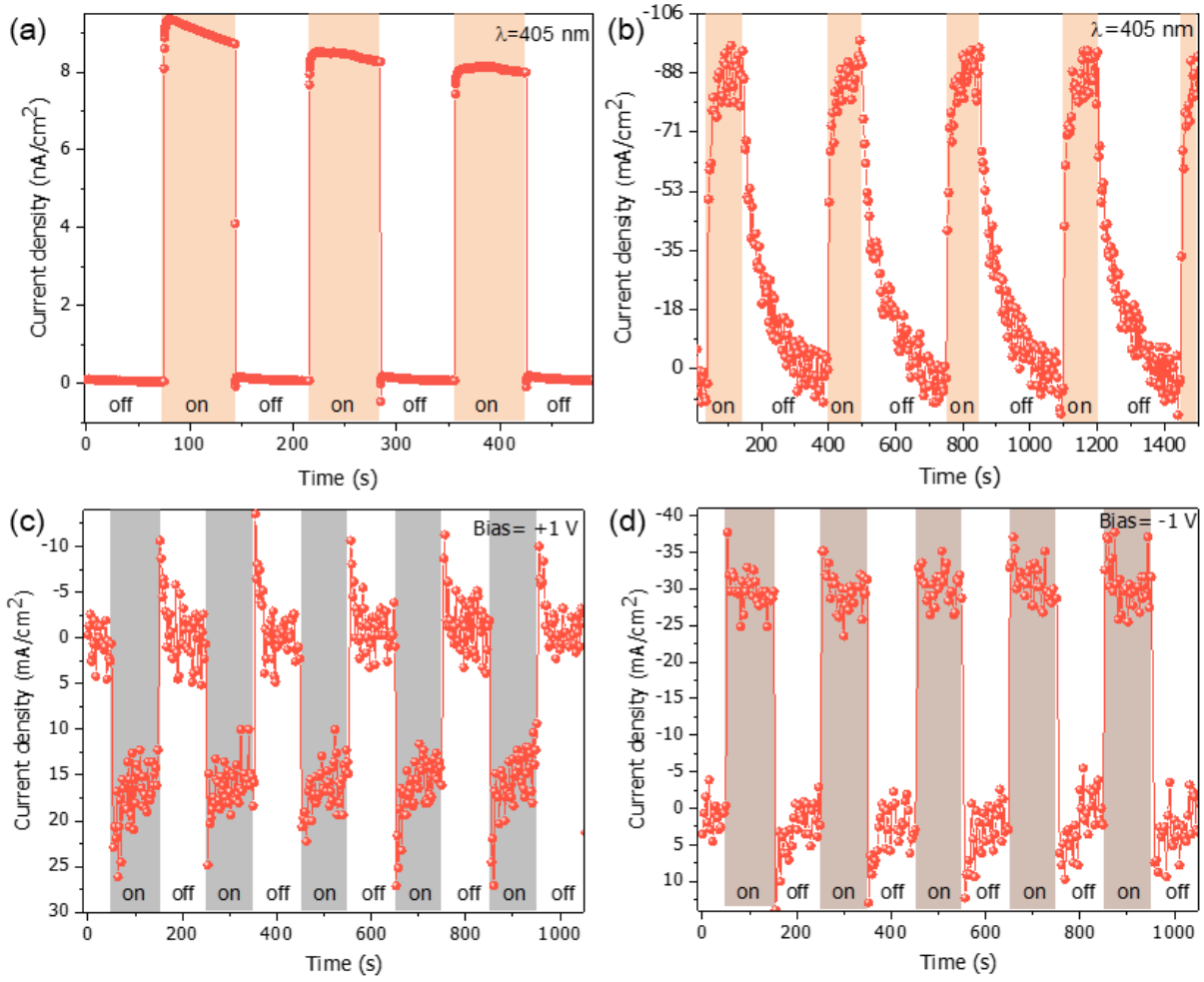

Figure 3: Light-induced changes in electronic properties. (a) Short circuit photocurrent density measured macroscopically with Au electrode on one side and ITO electrode on the other side. (b) Photocurrent density measured using AFM tip as one electrode while the Au electrode on other side of the sample. The laser spot was larger than the AFM tip, so the size of AFM tip can be considered as the effective area. An AC bias of 0.2V was applied for photocurrent measurement using AFM while no bias was applied for macroscopic measurement. Change in current density with applied bias of (c) + 1 V and (d) -1 V for the under the same conditions in which light was shined on the sample. Note the difference in the direction of increase in current density with light, positive bias and negative bias. Photo-response works analogous to applied negative bias.

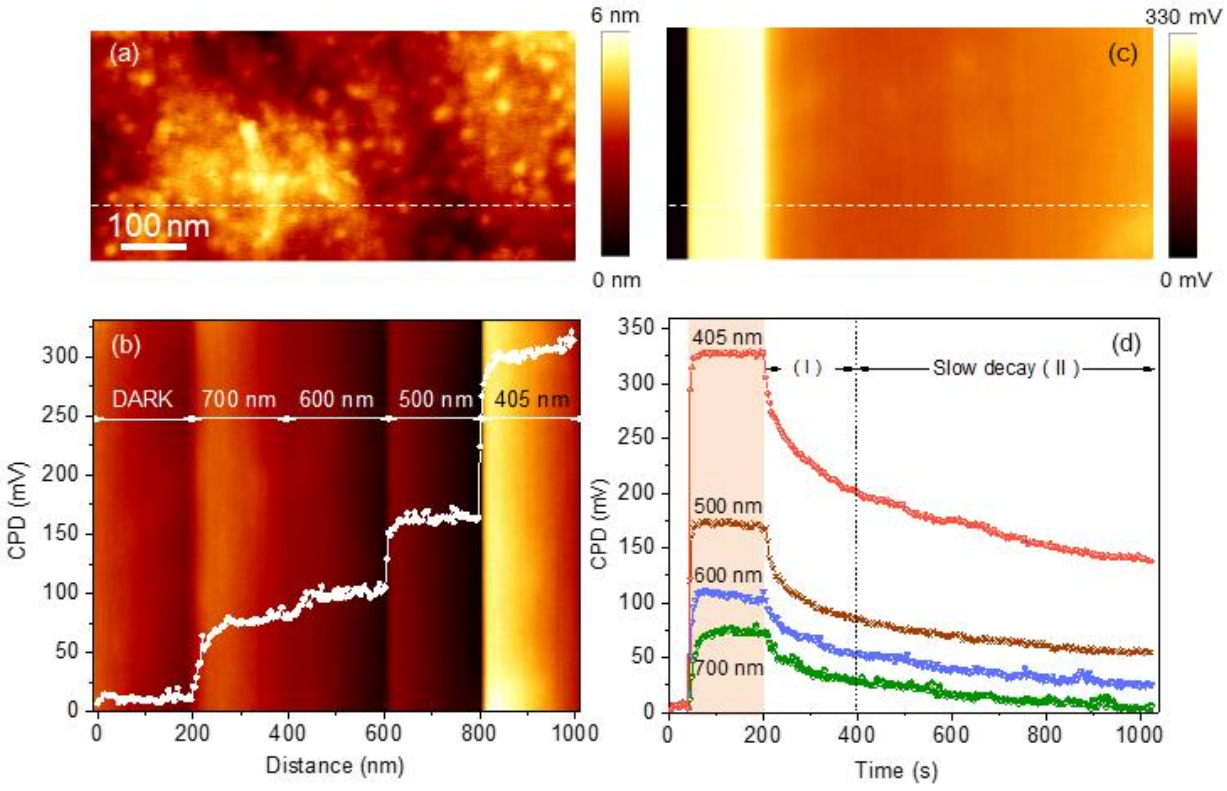

Figure 4: Surface potential changes with light illumination. (a) Topography of the KNN-BNNO surface. (b) KPFM image captured with different wavelengths of light superimposed on the contact potential difference (CPD) of the line profile highlighted in (a). (c) KPFM mapping of the CPD starting from the dark condition followed by the exposure to light of a particular wavelength (405nm, 500nm, 600nm, 700nm (only one at a time)) and CPD reversal on turning the light off. (d) Comparison of CPD rise and decay for different wavelengths corresponding to the line profile highlighted in (c). Shaded area in (d) denotes the period when the sample was exposed to the laser source. (I) and (II) indicates the sudden and slow decay zones.